MDPI

Article

Size-Dependent Strong Metal–Support Interactions of Rutile TiO$_2$-Supported Ni Catalysts for Hydrodeoxygenation of m-Cresol

Beilei Cui [1], Hua Wang [1], Qingfeng Ge [2] and Xinli Zhu [1,*]

1 Collaborative Innovation Center of Chemical Science and Engineering, Key Laboratory for Green Chemical Technology of Ministry of Education, School of Chemical Engineering and Technology, Tianjin University, Tianjin 300072, China
2 Department of Chemistry and Biochemistry, Southern Illinois University, Carbondale 62901, IL, USA
* Correspondence: xinlizhu@tju.edu.cn

Abstract: A series of rutile TiO$_2$-supported Ni catalysts with varying Ni sizes were prepared and reduced at 650 °C to explore the effect of Ni size on the strong metal–support interactions (SMSI) and its consequences on the hydrodeoxygenation (HDO) of m-cresol at 350 °C and atmospheric pressure. When the Ni size increases from 4 to 29.1 nm, the SMSI becomes stronger, e.g., the thickness of the TiO$_x$ overlayer and the coverage extent of TiO$_x$ on the Ni particle surface increase. Direct deoxygenation to toluene is the dominant pathway on Ni/TiO$_2$ catalysts with varying Ni loadings, with almost no CH$_4$ being formed. These results indicate that the TiO$_x$ overlayer significantly alters the property of Ni. That is, the C-C hydrogenolysis activity on bare Ni is completely inhibited due to SMSI, while the deoxygenation activity is improved at the Ni-TiO$_x$ interfacial perimeter sites. Meanwhile, the turnover frequency of HDO on small Ni particles of 4 nm is > 2 times higher than that on large Ni particles of 29.1 nm, indicating that the small Ni particle with moderate SMSI appears to be optimal for the direct deoxygenation of m-cresol to toluene. The results suggest HDO activity may be enhanced by tuning the metal particle size and SMSI degree.

Keywords: Ni/TiO$_2$; rutile; strong metal-support interactions; m-cresol; hydrodeoxygenation

1. Introduction

Oil, coal, and natural gas are not only non-renewable but also face shortages and depletion since energy consumption is ever-growing. At the same time, burning fossil fuels may cause environmental pollution, such as global warming, acid rain, and ozone layer depletion. Therefore, the development of clean and renewable energy sources instead of fossil fuels is the key to solving the energy problem. Fast pyrolysis effectively converts lignin biomass into phenolic-rich bio-oil [1–3], which can be converted to chemicals and fuel components by a hydrodeoxygenation (HDO) reaction [4–6]. Among different routes that likely happen during HDO, the direct deoxygenation (DDO) route consumes a minimal amount of H$_2$ and produces aromatics as important chemicals or fuel components. However, DDO is challenging due to the high energy barrier needed to break the C-O bond [7,8].

Strong metal–support interactions (SMSI) occur between the reducible metal oxide support and supported transition metal [9–13], which is manifested by the coverage of the transition metal surface by the partially reduced metal oxide after high-temperature hydrogen reduction, resulting in a reduced capacity for CO and H$_2$ chemisorption [14–18]. SMSIs have been extensively investigated, and generally, SMSIs are enhanced with an increase in the reduction temperature. Several works have investigated the effect of SMSIs on the hydrodeoxygenation of phenolic compounds [19–26]. For example, Zhao et al. [21]

demonstrated that stronger SMSIs of Pt/TiO$_2$ after reduction at 550 °C compared to reduction at 350 °C resulted in an increased turnover frequency (TOF) for the deoxygenation of m-cresol to toluene.

Generally, Ni catalysts show a high C-C hydrogenolysis activity at high temperatures and low pressure, producing large amounts of unfavorable CH$_4$ with high hydrogen consumption [27]. However, at low temperatures and high pressure, Ni catalysts readily hydrogenate the phenyl ring to produce saturated cycloalkanes [28,29]. The properties of metallic Ni can be modified by loading a second metal [30,31], adjusting the Ni particle size [32,33], and combining it with reducible metal oxide as support [34]. In particular, Zhang et al. [35] reported that the large Ni particles on anatase TiO$_2$ are encapsulated by TiO$_x$ after reduction temperatures of > 300 °C and therefore lose activity toward HDO due to the SMSI. In contrast, the highly dispersed Ni atomic clusters inhibit TiO$_x$ encapsulation by interaction with the defective sites of anatase TiO$_2$ and thus improve the selectivity of phenol during HDO of guaiacol. Nevertheless, the authors stated that it could not be excluded that the high selectivity may be attributed to small Ni particles partially covered by TiO$_x$.

Many reports have explored the effect of metal particle size on the HDO of phenolic compounds. On an inert support of SiO$_2$, the change in particle size reflects the nature of a metal. Mortensen et al. [32] found that phenol is readily hydrogenated to cyclohexanol on large Ni particles at 275 °C and 100 bar, while the small Ni particles have a high TOF of deoxygenation to cyclohexane due to more step sites. Our previous HDO work at a low pressure and vapor phase [36] showed that small Ni particles favor deoxygenation of m-cresol to toluene due to more step and corner sites, while large Ni particles favor C-C hydrogenolysis toward CH$_4$ due to more terrace sites. On the other hand, the effect of metal particle size on the HDO activity on a reducible metal oxide support is likely dependent on the synergistic effect of the metal and the support. Mao et al. [37] demonstrated that as the Au particle size is increased from 3 to 41 nm, the conversion of guaiacol decreases from 65 to 36%, resulting from the smaller interfacial area between anatase TiO$_2$ and large Au particles. Similarly, by adjusting the Ru particle size on Ru/TiO$_2$, Otomoso et al. [38] found that the activity of m-cresol deoxygenation to toluene is related to the interfacial perimeter of Ru and TiO$_2$. Despite the fact that it has been reported that the SMSI is more pronounced on larger metal particles [39], metal-particle-size-dependent SMSI have rarely been explored for the HDO of phenolics.

In our recent work [40], we compared the effects of the TiO$_2$ crystalline phase and reduction temperature on the HDO of m-cresol. Anatase TiO$_2$ is more readily reduced, resulting in a higher and thicker TiO$_x$ coverage on the Ni particle and, therefore, a stronger SMSI at temperatures > 350 °C, which, however, led to decreased HDO activity due to excessive SMSIs. Very differently, rutile TiO$_2$ is less reducible. A moderate (optimal) SMSI could only be achieved on Ni/r-TiO$_2$ when the reduction temperature was increased to 650 °C, resulting in the highest activity for HDO. More importantly, the selectivity of direct deoxygenation reached 84.8% at 100% m-cresol conversion. However, the effect of Ni particle size on the SMSI of Ni/TiO$_2$ for HDO was not explored in that study.

In this study, we prepared a series of rutile TiO$_2$-supported Ni catalysts with various Ni sizes by tuning the amount of Ni loadings. The relationship between Ni particle size and the degree of the SMSI was investigated, and the consequences on the HDO of m-cresol were elucidated. The results showed that the SMSI is dependent on the Ni particle size, and the larger the Ni particle size, the stronger the SMSI. The coverage of the Ni surface by TiO$_x$ improves the deoxygenation of m-cresol to toluene while inhibiting C–C hydrogenolysis toward CH$_4$. Moreover, the TOF of HDO on a small Ni size of 4 nm is >2 times higher than that on a large Ni size of 29.1 nm due to the moderate SMSI.

2. Results and Discussion

2.1. Catalyst Characterization

Figure 1 shows the XRD patterns of Ni/TiO_2 catalysts with varying amounts of Ni loadings. Only the rutile phase of TiO_2 is identified for all samples, indicating no TiO_2 phase transition takes place after reduction at 650 °C. No diffractions of Ni species are observed for $1Ni/r\text{-}TiO_2$, which suggests Ni is highly dispersed, while metallic Ni diffractions at 2θ of 44.41° and 51.85° are observed for $5Ni/r\text{-}TiO_2$ and $10Ni/r\text{-}TiO_2$, which correspond to Ni(111) and (200), respectively. It is evident that the diffraction peak of Ni(111) becomes stronger and sharper with increasing Ni loadings (see inset), pointing to the fact that high Ni loading leads to the agglomeration of Ni particles. According to the Scherrer formula, the average Ni particle sizes of $5Ni/r\text{-}TiO_2$ and $10Ni/r\text{-}TiO_2$ are estimated to be 17.2 and 23.1 nm, respectively.
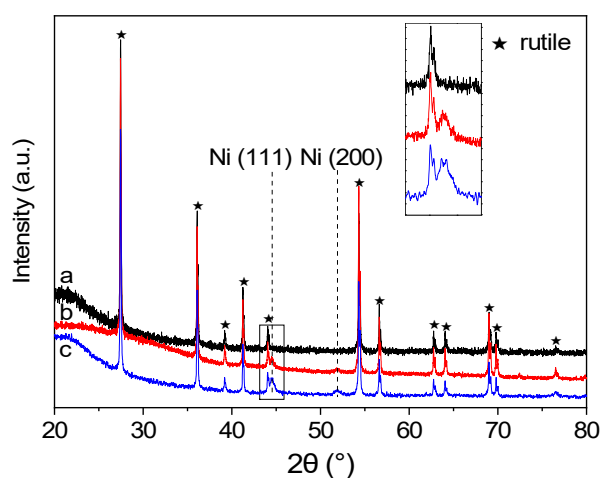

Figure 1. XRD patterns of 650 °C reduced (**a**) $1Ni/r\text{-}TiO_2$, (**b**) $5Ni/r\text{-}TiO_2$, and (**c**) $10Ni/r\text{-}TiO_2$.

H_2-TPR is used to probe the interaction between Ni and rutile TiO_2. As shown in Figure 2, the bare rutile TiO_2 consumes few H_2 at high reduction temperatures. A reduction peak at 494 °C is observed for $1Ni/r\text{-}TiO_2$, which is attributed to the reduction of small Ni particles strongly interacting with $r\text{-}TiO_2$. As the amount of Ni loading is increased, another peak emerges at lower temperatures, which can be ascribed to the reduction of larger Ni particles with weaker interaction with $r\text{-}TiO_2$. This peak increases in intensity and shifts to lower temperatures from 387 to 378 °C with increasing Ni loadings from 5% to 10%, indicating larger NiO particles are present for $10Ni/r\text{-}TiO_2$. The quantified hydrogen consumption is summarized in Table 1. It is evident that the H_2/Ni molar ratio is higher than 1 for all samples, indicating besides the complete reduction of NiO, the $r\text{-}TiO_2$ support is also partially reduced. This phenomenon is related to the spillover of H from metallic Ni to TiO_2 support, resulting in a partial reduction of TiO_2 in proximity to Ni. It is important to note that the H_2/Ni molar ratio is the highest on $1Ni/r\text{-}TiO_2$ (1.41) and decreases with increasing Ni loadings, which suggests that a smaller Ni particle favors more H_2 spillover due to high Ni dispersion.

The representative TEM images of $1Ni/r\text{-}TiO_2$, $5Ni/r\text{-}TiO_2$, and $10Ni/r\text{-}TiO_2$ are shown in Figure 3. The number-weighted-average Ni particle size is 4 nm for $1Ni/r\text{-}TiO_2$ and increases to 23.8 and 29.1 nm for $5Ni/r\text{-}TiO_2$ and $10Ni/r\text{-}TiO_2$, respectively (Table 2), which are in good agreement with the XRD results. The Ni dispersion was measured by CO chemisorption. As shown in Table 2, the dispersion of Ni decreases from 1.03 to 0.6% with increasing Ni loadings. It is important to note that the CO chemisorption-measured Ni dispersions are much lower than those estimated from Ni particle size (Table 2). Such a difference points to the occurrence of an SMSI. That is, the spillover H from Ni reduces the adjacent TiO_2, and then the partially reduced TiO_x (x < 2) migrates onto the surface of the

Ni particle to form an overlayer, which leads to a decrement in the accessibility of surface Ni by CO.
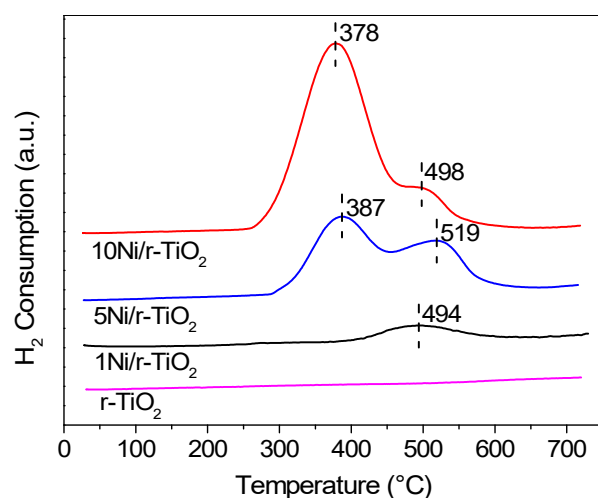
Figure 2. H_2-TPR profiles for 1Ni/r-TiO$_2$, 5Ni/r-TiO$_2$, 10Ni/r-TiO$_2$, and r-TiO$_2$ catalysts.

Table 1. H_2 consumption and molar ratio of H_2/Ni over 1Ni/r-TiO$_2$, 5Ni/r-TiO$_2$, and 10Ni/r-TiO$_2$ catalysts determined by H_2-TPR.

Sample	H$_2$ Consumption		H$_2$/Ni
	Total (mmol·g^{-1})	Ni (mmol·g^{-1}) [a]	
1Ni/r-TiO$_2$	0.024	0.017	1.41
5Ni/r-TiO$_2$	0.096	0.084	1.14
10Ni/r-TiO$_2$	0.175	0.166	1.05

[a] H_2 consumption for the complete reduction of NiO to Ni according to the theoretical stoichiometric ratio.
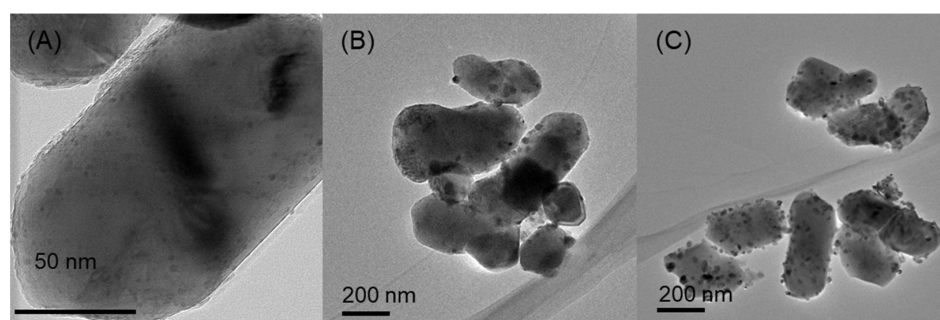
Figure 3. TEM images of 650 °C reduced (**A**) 1Ni/r-TiO$_2$, (**B**) 5Ni/r-TiO$_2$, and (**C**) 10Ni/r-TiO$_2$ catalysts.

Table 2. Ni particle size and dispersion of 1Ni/r-TiO$_2$, 5Ni/r-TiO$_2$, and 10Ni/r-TiO$_2$ catalysts.

Sample	Metal Ni d$_{XRD}$ [a] (nm)	Metal Ni d$_{TEM}$ [b] (nm) [a]	Metal Ni Dispersion [b] (%)	Metal Ni Dispersion [c] (%)
1Ni/r-TiO$_2$	—	4.0	25	1.03
5Ni/r-TiO$_2$	17.2	23.8	4.3	0.76
10Ni/r-TiO$_2$	23.1	29.1	3.5	0.60

[a] Particle size was derived from XRD; [b] Particle size was measured by counting > 200 Ni particles in the TEM and estimating the Ni dispersion (dispersion = 1.01/d$_{TEM}$ [41]); [c] Ni dispersion achieved by CO chemisorption.

High-resolution (HR) TEM observations were used to visualize the degree of SMSI as a function of Ni particle size (Figure 4) since it has been reported that the SMSI is sensitive to the metal particle size [39]. As shown in Figure 4A,B, a small 5 nm Ni particle (d$_{200}$ = 0.180 nm) is located on the surface of TiO$_2$ for 1Ni/r-TiO$_2$. Interestingly, this particle

is partially covered by a thin TiO_x overlayer of ~0.4 nm. The extent of coverage increases and the overlayer becomes thicker with an increase in the Ni particle size. For $5Ni/r-TiO_2$ (Figure 4C,D), a TiO_x overlayer of ~0.64 nm partially covers a Ni particle (d_{111} = 0.204 nm) of ~10 nm. The TiO_x overlayer thickens further to ~1.37 nm for $10Ni/r-TiO_2$ and appears to completely encapsulate a Ni particle of ~20 nm (Figure 4E,F).
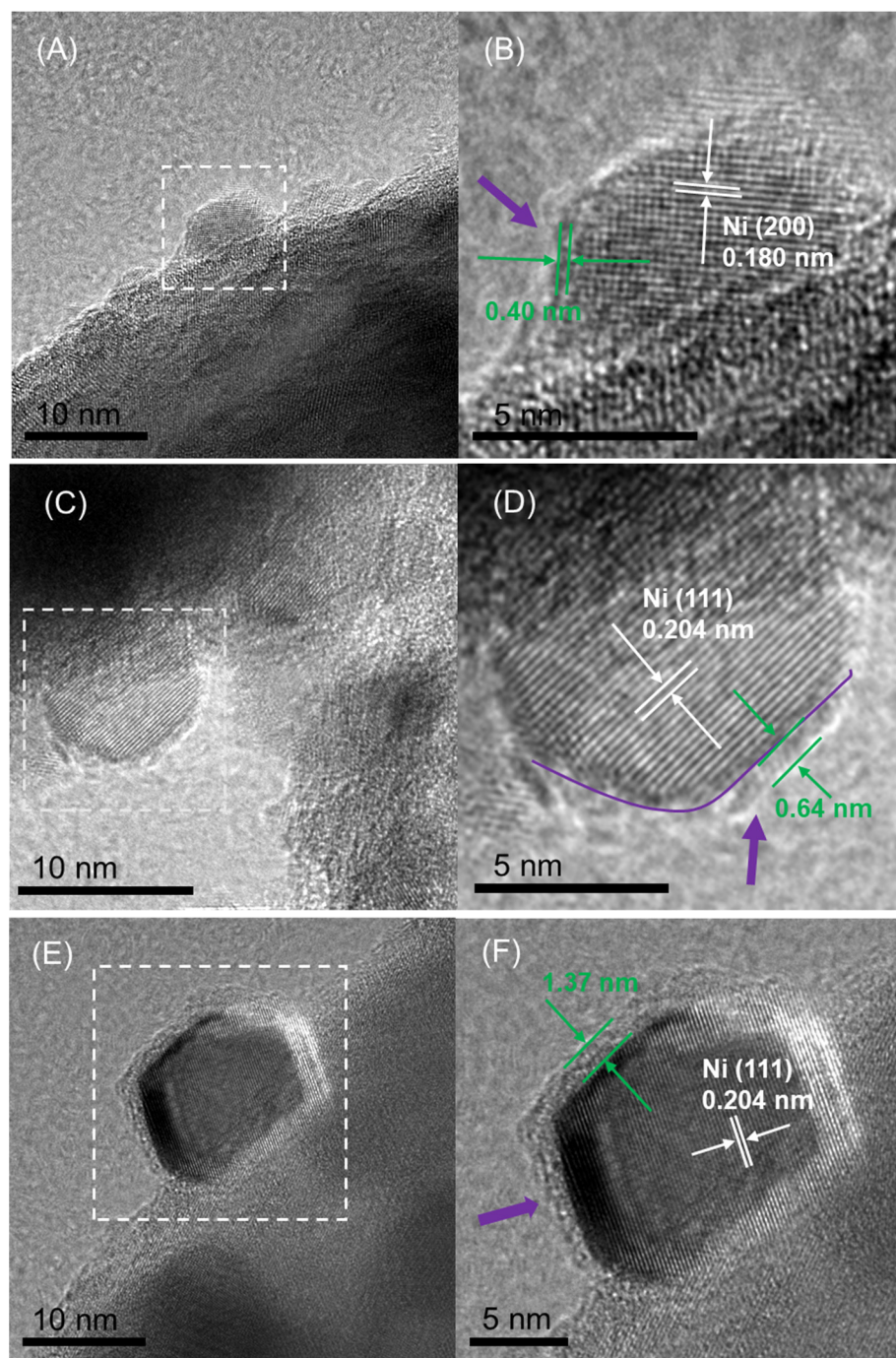
Figure 4. HR-TEM images of 650 °C-reduced (**A,B**) $1Ni/r-TiO_2$, (**C,D**) $5Ni/r-TiO_2$, and (**E,F**) $10Ni/r-TiO_2$. The white line indicates the lattice stripes of Ni(111) and Ni(200), and the purple arrow highlights the TiO_x overlayer and marks its thickness with a green line.

The electronic structure of $Ni/r-TiO_2$ catalysts was explored by XPS. Figure 5 shows the Ni 2p and Ti 2p spectra of $Ni/r-TiO_2$ samples with different Ni loadings. For $1Ni/r-TiO_2$, the binding energy of Ni^0 is at 852.4 eV, while the binding energies of Ni^{2+} and the

satellites of Ni^{2+} are at 856 and 861.7 eV, respectively (Figure 5A). As the samples were reduced ex situ; the Ni surface was partially oxidized when transferring the sample to the XPS chamber. Compared to $1Ni/r\text{-}TiO_2$, the binding energy of Ni^0 for $5Ni/r\text{-}TiO_2$ and $10Ni/r\text{-}TiO_2$ shifts to lower values by 0.2 eV and 0.4 eV, respectively. One may expect the increased Ni encapsulation by TiO_x with increasing Ni loadings (see Figure 4) results in more electron transfer from oxygen vacancies ($O_v\text{-}Ti^{3+}$) to Ni, producing electron-rich Ni^0. In addition, the Ni^0/Ni^{2+} ratio rises from 0.09 to 0.22 with an increase in Ni loading (Table 3). This likely resulted from stronger SMSIs, i.e., more encapsulation of Ni by TiO_x for the $10Ni/r\text{-}TiO_2$ sample, which prevented the oxidation of surface Ni during exposure to air. On the other hand, the peak of Ti^{3+} is tiny relative to that of Ti^{4+} for all samples (Figure 5B), reflecting that rutile TiO_2 is difficult to be reduced. Additionally, the Ti^{3+}/Ti^{4+} ratio increases with increasing Ni loadings (Table 3), which indicates more of the Ti species was reduced at higher Ni loadings.
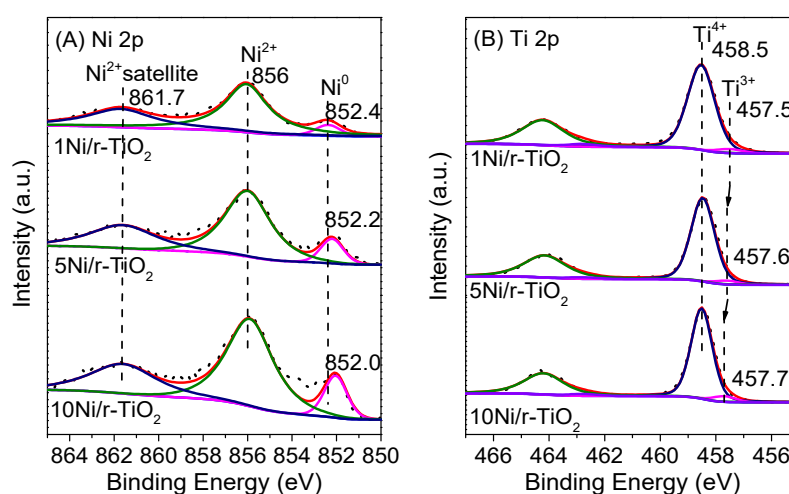

Figure 5. (**A**) Ni 2p and (**B**) Ti 2p XPS spectra of 650 °C-reduced $1Ni/r\text{-}TiO_2$, $5Ni/r\text{-}TiO_2$, and $10Ni/r\text{-}TiO_2$.

Table 3. The XPS-derived Ni^0/Ni^{2+} and Ti^{3+}/Ti^{4+} ratios.

Sample	Ni^0/Ni^{2+}	Ti^{3+}/Ti^{4+}
$1Ni/r\text{-}TiO_2$	0.09	0.03
$5Ni/r\text{-}TiO_2$	0.17	0.04
$10Ni/r\text{-}TiO_2$	0.22	0.06

2.2. Catalytic Performance

The activities of bare supports (SiO_2 and $r\text{-}TiO_2$) and supported Ni catalysts ($1Ni/SiO_2$ and $1Ni/r\text{-}TiO_2$) in the HDO of m-cresol were compared at 350 °C and W/F of 2 h. As shown in Figure 6, the bare supports are inactive for HDO m-cresol (conversion < 1%), while the supported Ni catalysts are active for the HDO reaction. The type of support plays a crucial role in the major product distributions. The major product over $1Ni/SiO_2$ is phenol (Ph). CH_4 and deoxygenation products of benzene (Ben) and toluene (Tol) are the minor products. Consistent with previous work [27], the results indicate that the metallic Ni favors the C-C hydrogenolysis reaction over the deoxygenation reaction under the current reaction condition. In contrast to $1Ni/SiO_2$, although the conversion is slightly lower, Tol and dimethylbiphenyl (DMB) are the major products on $1Ni/r\text{-}TiO_2$. More importantly, almost no CH_4 is formed. This result highlights that the combination of reducible $r\text{-}TiO_2$ and Ni provides a unique catalytic activity for the direct deoxygenation of m-cresol to Tol. The TiO_x overlayer on the Ni surface inhibits the C-C hydrogenolysis activity on the metallic Ni, and the $Ni\text{-}TiO_x$ interfacial site enhances the deoxygenation activity.
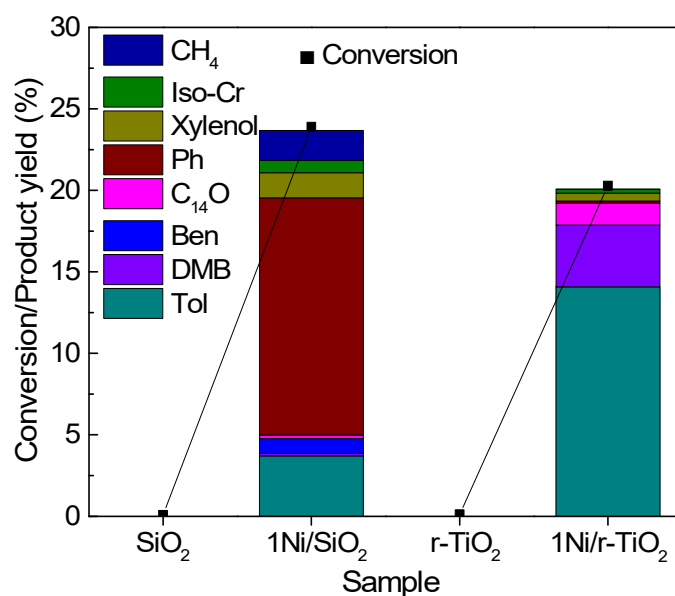
Figure 6. m-Cresol conversion and major product yields and on bare supports (SiO$_2$ [31] and r-TiO$_2$) and supported Ni catalysts (1Ni/SiO$_2$ and 1Ni/r-TiO$_2$). Reaction conditions: T = 350 °C, P = 1 atm, H$_2$/m-cresol = 50, TOS = 30 min, W/F = 2 h. Product with a yield of less than 0.2% is not listed. Ben, Tol, Iso-Cr, Ph, DMB, and C$_{14}$O represent benzene, toluene, cresol isomers, phenol, dimethylbiphenyl, and 5,5'-dimethyl-3-hydroxybiphenyl, respectively.

The effect of Ni loadings on Ni/r-TiO$_2$ was then investigated for m-cresol HDO at 350 °C and W/F of 2 h. As the Ni loading is increased from 1% to 10%, m-cresol conversion increases from 20.3% to 54.5% (Figure 7). The Tol yield and the total aromatics yield (Ben, Tol, and DMB) follow the same trend. Previous work of HDO on Ni/SiO$_2$ under similar reaction conditions showed that when the Ni particle size increases from 2 to 22 nm, the selectivity toward C-C hydrogenolysis increases while selectivity toward deoxygenation decreases [36]. In the present work, almost no CH$_4$ is produced on 10Ni/r-TiO$_2$ despite the Ni particle size being as large as 29.1 nm. This difference suggests that Ni particle size on Ni/r-TiO$_2$ is not the dominant factor that determines product distribution. In contrast, the SMSI appears to be the key to tune the reaction pathway from hydrogenolysis to direct deoxygenation.

To further compare the effect of Ni particle size, the conversion of m-cresol and the evolution of major product yields as a function of W/F were studied. As illustrated in Figure 8, Tol is always the dominant product at all conversion levels, irrespective of different Ni particle sizes. In addition, the yield of CH$_4$ is near zero. This result indicates that SMSI changes the properties of the Ni surface. That is, the TiO$_x$ overlayer inhibits the C–C hydrogenolysis activity and increases the deoxygenation activity at the interfacial of Ni–TiO$_x$. The yield of DMB decreases while the yield of xylenols increases with an increase in Ni particle size from 1Ni/r-TiO$_2$ to 10Ni/r-TiO$_2$ (Figure 8B–D). The formation of DMB is completed through the hydrogenation of m-cresol on Ni to methylcyclohexanone (MCHone) and methylcyclohexanol (MCHol), which condense to 5,5´-dimethyl-3-hydroxybiphenyl (C$_{14}$O) on the acid site and then subsequently deoxygenate to DMB (see Figure 9). The xylenols/phenol and cresol isomers (Iso-Cr) are formed through the disproportionation and isomerization of m-cresol on the acidic site [42], respectively (see Figure 9). The trend of increased xylenols at the expense of DMB with an increase in Ni size likely resulted from stronger acid sites of Ti^{3+} [43] being produced on the catalysts with higher Ni loadings.
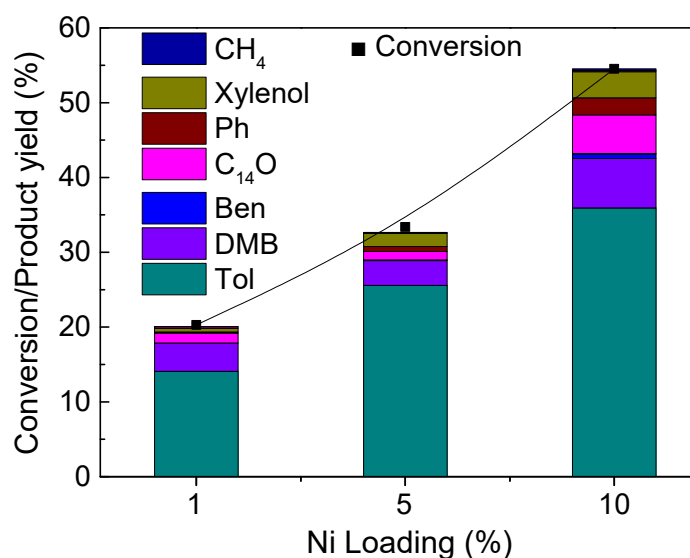
Figure 7. m-Cresol conversion and major product yields with varying Ni loadings on r-TiO$_2$. Reaction conditions: T = 350 °C, P = 1 atm, H$_2$/m-cresol = 50, TOS = 30 min, W/F=2 h. Product with a yield of less than 0.2% is not listed. Ben, Tol, Ph, DMB, and C$_{14}$O represent benzene, toluene, phenol, dimethylbiphenyl, and 5,5´-dimethyl-3-hydroxybiphenyl, respectively.
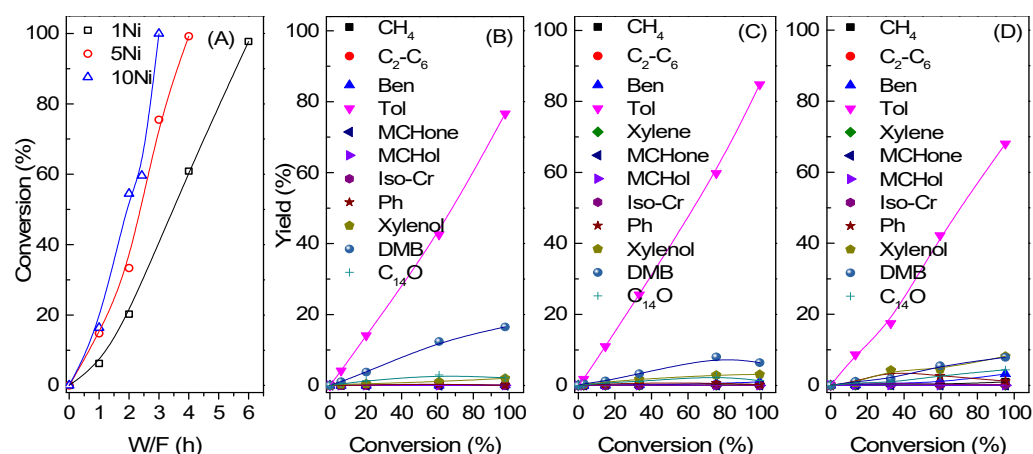
Figure 8. Conversion rate as a function of W/F (**A**) and product yields with change in conversion over (**B**) 1Ni/r-TiO$_2$, (**C**) 5Ni/r-TiO$_2$, and (**D**) 10Ni/r-TiO$_2$. Reaction conditions: T=350 °C, P = 1 atm, H$_2$/m-cresol = 50, TOS = 30 min. Ben, Tol, MCHone, MCHol, Iso-Cr, Ph, DMB, and C$_{14}$O represent benzene, toluene, methylcyclohexanone, methylcyclohexanol, cresol isomers, phenol, dimethylbiphenyl, and 5,5´-dimethyl-3-hydroxybiphenyl, respectively.

Table 4 compares the selectivity of the products at the near-complete conversion of m-cresol on three catalysts. The selectivity of aromatics (Tol, Ben, Xylene, and DMB) decreases slightly from 95.4% for 1Ni/r-TiO$_2$ to 92.9% for 5Ni/r-TiO$_2$ and then decreases significantly to 83.2% for 10Ni/r-TiO$_2$. The total selectivity of the products generated on the acidic sites (C$_{14}$O, Ph, Xylenol, and Iso-Cr) shows an opposing trend. That is, the selectivity increases from 4.4% on 1Ni/r-TiO$_2$ to 14.7% on 10Ni/r-TiO$_2$. This trend likely reflects that more Ti^{3+} cations are formed by spillover H from Ni at high Ni loadings.
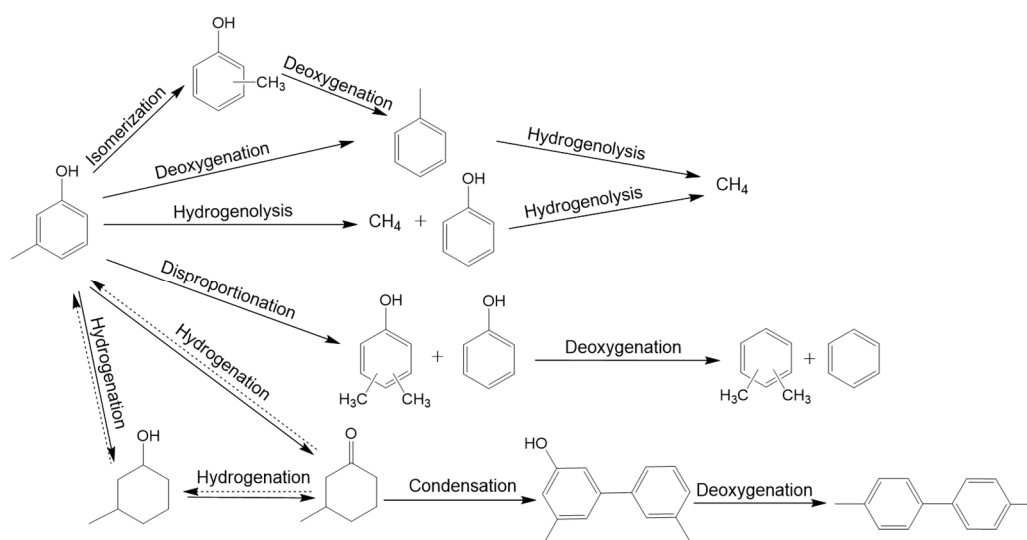
Figure 9. Proposed major reaction pathway during hydrodeoxygenation on Ni/r-TiO$_2$ catalysts.

Table 4. Product yields at near-complete conversion of m-cresol over 1Ni/r-TiO$_2$, 5Ni/r-TiO$_2$, and 10Ni/r-TiO$_2$.

Catalyst	1Ni/r-TiO$_2$	5Ni/r-TiO$_2$	10Ni/r-TiO$_2$
W/F	6	4	3
Conversion(%)	97.75	99.25	95.2
Selectivity(%)			
Tol	78.37	85.41	71.46
DMB	16.89	6.47	8.32
Ben	0.13	1.01	3.37
Xylene	0	0.05	0
C$_{14}$O	2.20	1.58	4.60
Ph	0.07	0.26	1.30
Xylenol	2.05	3.63	8.63
Iso-Cr	0.04	0.01	0.19
MCHone	0	0	0
MCHol	0.04	0	0
C$_2$-C$_6$	0.02	0.07	0.27
CH$_4$	0.02	0.23	1.01

Reaction conditions: T = 350 °C, P = 1 atm, H$_2$/m-cresol = 50, TOS = 30 min, W/F was adjusted to obtain a similar conversion of m-cresol.

The intrinsic m-cresol conversion rates, Tol, and total aromatic formation rates were measured at conversions < 10%. As reported in Table 5, the conversion and Tol formation rates increase significantly from 9.66 and 6.33 μmol·g^{-1}·min^{-1} for 1Ni/r-TiO$_2$ to 23.45 and 15.69 μmol·g^{-1}·min^{-1} for 5Ni/r-TiO$_2$, respectively. However, these rates increase only slightly when the Ni loading is further increased by 10%. In contrast, a reverse trend is found for the TOF, which is estimated using the Ni dispersion measured by CO chemisorption. The TOFs of both m-cresol conversion and Tol formation are the highest on 1Ni/r-TiO$_2$ with a small Ni size of 4 nm, and these values decrease gradually with increasing Ni loadings (or Ni particle size). Specifically, the TOFs on 1Ni/r-TiO$_2$ (Ni size of 4 nm) are > 2 times higher than those on 10Ni/r-TiO$_2$ (Ni size of 29.1 nm). These results indicate that a small Ni size with a moderate extent of SMSI is more active for the deoxygenation of m-cresol. On the one hand, the small Ni particle itself is more active in the HDO reaction [36,38]. On the other hand, too strong of an SMSI encapsulates the Ni particle too much and therefore modifies the property of Ni. Consequently, the hydrogenation ability of Ni may be lowered, which eventually lowers the TOF.

Table 5. The intrinsic reaction rate and turnover frequency (TOF) for HDO of m-cresol.

Sample	Reaction Rate ($\mu mol \cdot g^{-1} \cdot min^{-1}$) [a]			Turnover Frequency (min^{-1}) [a]		
	m-cresol	Tol	Deoxygenation [b]	m-cresol	Tol	Deoxygenation [b]
1Ni/r-TiO$_2$	9.66	6.33	7.25	5.55	3.64	4.16
5Ni/r-TiO$_2$	23.45	15.69	17.26	3.64	2.43	2.68
10Ni/r-TiO$_2$	25.39	15.83	17.95	2.48	1.54	1.75

[a] Measured at conversion < 10%. Reaction conditions: T = 350 °C, P = 1 atm, H$_2$/m-cresol = 50, TOS = 30 min;
[b] Deoxygenation represents aromatics products (benzene, toluene, and DMB).

At a high reduction temperature of 650 °C, Ni is partially covered by reduced TiO$_x$, forming the Ni-TiO$_x$ interfacial sites. Compared with Ni/SiO$_2$, the TiO$_x$ overlayer on Ni/r-TiO$_2$ improves the direct deoxygenation activity, making Tol the major product. This can be explained by the adsorption of oxygen atoms of m-cresol at oxygen vacancies and the adsorption of a phenyl ring on Ni, which facilitates the C-O breakage [44]. In addition, the degree of SMSI is closely related to the Ni particle size. The thickness of the TiO$_x$ overlayer and its coverages on the Ni surface increase as the Ni particle size is increased (Figure 4). Too much coverage of TiO$_x$ on large Ni particles at high loadings reduces the surface Ni that is accessible by m-cresol, which eventually reduces the activity in HDO. As the Ni loading increases, more TiO$_2$ is reduced (see XPS results), resulting in increased acid-catalyzed reactions, such as disproportionation. In summary, a small Ni particle with moderate SMSI appears to be optimal for the direct deoxygenation of m-cresol to toluene.

As shown in Figure 10, the three catalysts showed a similar deactivation trend with time on stream. The conversion decreased rapidly in the first 2 h, and then the deactivation became very slow. It is important to note that Tol is always the dominant product, which likely indicates the deactivation is due to the loss of the number of active sites.
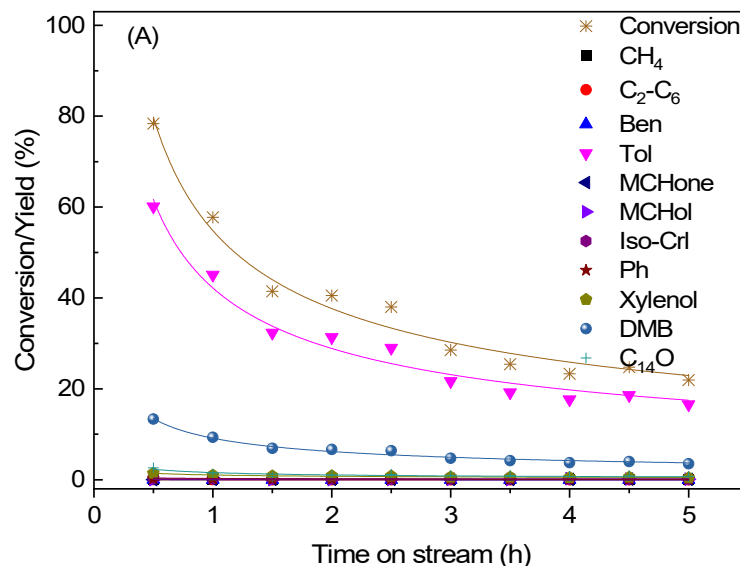
Figure 10. *Cont.*
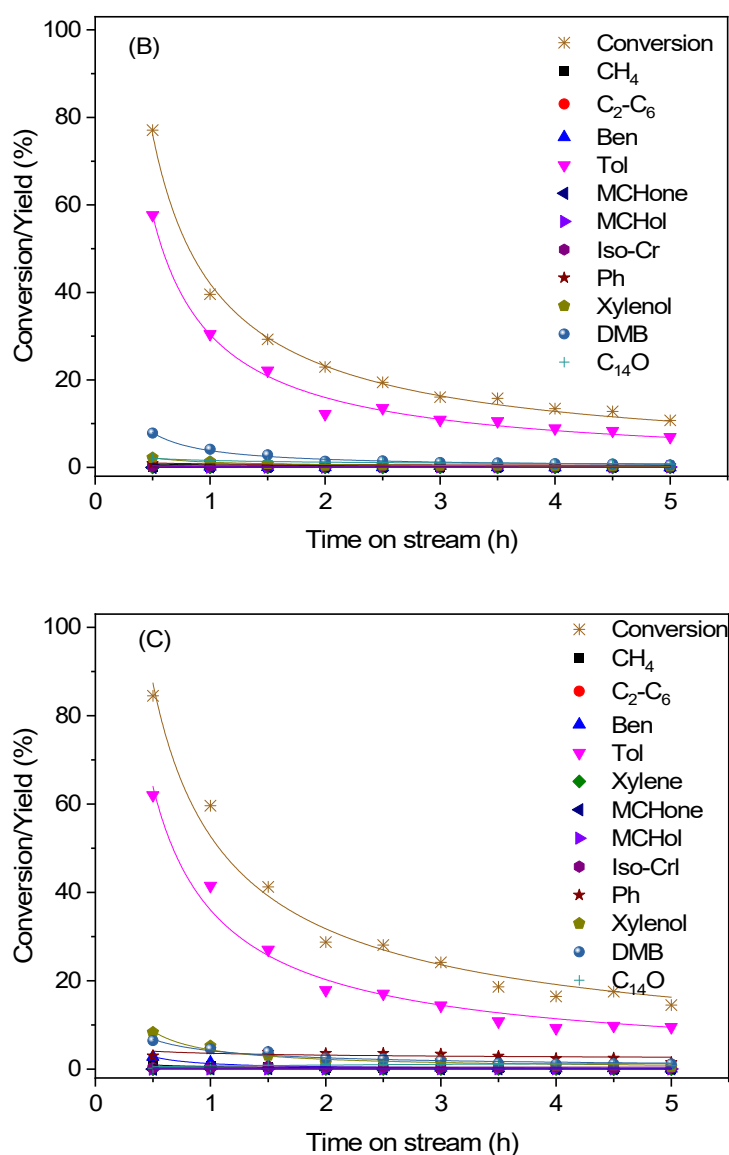
Figure 10. Stability of (A) 1Ni/r-TiO$_2$-H650, (B) 5Ni/r-TiO$_2$-H650, and (C) 10Ni/r-TiO$_2$-H650 catalysts during HDO of m-cresol. Reaction conditions: T = 350 °C, P = 1 atm, H$_2$/m-cresol = 50. W/F in the figure are: (**A**) 5 h, (**B**) 3 h, and (**C**) 2.7 h, respectively. Ben, Tol, MCHone, MCHol, Iso-Cr, Ph, DMB, and C$_{14}$O represent benzene, toluene, methylcyclohexanone, methylcyclohexanol, cresol isomers, phenol, dimethylbiphenyl, and 5,5′-dimethyl-3-hydroxybiphenyl, respectively.

3. Experimental

3.1. Catalyst Preparation

Catalysts with varying amounts of Ni loadings were prepared using an incipient wetness impregnation method. Rutile TiO$_2$ (r-TiO$_2$, 99.8%, 13.9 m^2/g Macklin, Shanghai, China) was added to a Ni(NO$_3$)$_2$·6H$_2$O (Aladdin, Shanghai, China, 98%) precursor solution, after which the samples were aged at room temperature for 12 h and dried at 100 °C for 12 h. All catalysts were calcined at 400 °C for 4 h at a ramping rate of 2 °C/min. The catalysts were named xNi/r-TiO$_2$, where x (x = 1, 5, and 10) is the mass fraction (%) of Ni in the catalysts.

3.2. Catalyst Characterization

X-ray diffraction (XRD) was measured on a Rigaku D/max 2500 (JEOL, Tokyo, Japan) diffractometer using Cu Kα as the radiation source. The 2θ angle range of the scan is 20–80°, and the scanning rate is 6°/min. The transmission electron microscopy (TEM) observation

of the samples was performed in a JEM-F200 electron microscope (JEOL, Tokyo, Japan) at 200 KV. Approximately 200 particles were analyzed to calculate the average particle size of Ni. Hydrogen temperature-programmed reduction (H_2-TPR) of the catalysts was measured on a Chemisorb 2750 (Micrometrics, Atlanta, GA, USA). A catalyst sample of 100 mg was charged in a U-shaped quartz tube, pretreated by purging in flowing N_2 for 1 h at 300 °C, and was finally cooled to room temperature. The sample was heated from room temperature to 800 °C in 10% H_2/Ar at a rate of 10 °C/min. The consumption of H_2 during TPR was monitored via a TCD detector. The amount of H_2 consumed was calibrated by a reduction of a known amount of CuO. The stoichiometric H_2/NiO ratio was assumed as 1 to estimate the theoretical H_2 needed for complete reduction of NiO. The CO chemisorption was measured in the same equipment used for H_2-TPR. The catalyst was reduced at 650 °C for 1 h, followed by purging by flowing He for 30 min and finally cooling to room temperature. After the baseline was stabilized, pulses of 5% CO/He (500 μL) were sent onto the sample until a constant CO peak was achieved. The stoichiometric CO/Ni ratio was assumed as 1 to estimate the dispersion of Ni. The X-ray photoelectron spectra (XPS) of the samples were recorded on a PHI 1600 ESCA spectrometer (Chanhassen, MN, USA) fitted with an Al Kα (1486.6 eV) radiation source and were calibrated with the C1s peak at 284.8 eV.

3.3. Catalytic Activity Measurement

The vapor-phase HDO of m-cresol was performed in fixed-bed reactor at 350 °C and atmospheric pressure. Prior to reaction, the catalyst was reduced in situ with flowing hydrogen (28 mL/min) at 650 °C for 1 h since previous work showed that this reduction condition resulted in optimal SMSI for rutile support. m-Cresol was injected into the reactor by a syringe pump (KDS100, KD scientific). The reactant was vaporized at the injection port before entering the reactor. The molar ratio of H_2/m-cresol was maintained at 50 for all runs. The products were quantified online using a gas chromatograph (GC, 7890B, Agilent, Santa Clara, CA, USA). All lines were wrapped with heating tape and kept at 230°C to ensure no condensation. Space time (W/F, h) was defined as the ratio of weight of catalyst (g) to the organic feed flow rate (g/h).

4. Conclusions

We prepared a series of Ni/r-TiO$_2$ catalysts with different Ni particle sizes by varying the amount of Ni loadings. These catalysts were reduced at 650 °C and tested at 350 °C and atmospheric pressure for hydrodeoxygenation of m-cresol. The particle size dependence of SMSI was observed. A small Ni size of 4 nm resulted in a thin and partial TiO$_x$ coverage; however, a large Ni particle of 29.1 nm led to a thick and almost complete TiO$_x$ coverage. The SMSI inhibited the C-C hydrogenolysis reaction of Ni while promoting the direct deoxygenation activity at the Ni-TiO$_x$ interfacial site. The TOF of deoxygenation to toluene on 1Ni/r-TiO$_2$ with 4 nm Ni is > 2 times higher than that on 10Ni/r-TiO$_2$ with 29.1 nm Ni. This result indicates that a small Ni particle with a moderate SMSI appears to be optimal for the direct deoxygenation of m-cresol to toluene.

Author Contributions: Investigation, data curation, and writing-original draft, B.C.; validation, H.W. and Q.G.; Conceptualization, validation, resources, writing-review and editing, supervision, and funding acquisition, X.Z. All authors have read and agreed to the published version of the manuscript.

Data Availability Statement: Data will be made available upon request.

Conflicts of Interest: The authors declare no conflict of interest.

References

1. Anex, R.P.; Aden, A.; Kazi, F.K.; Fortman, J.; Swanson, R.M.; Wright, M.M.; Satrio, J.A.; Brown, R.C.; Daugaard, D.E.; Platon, A.; et al. Techno-economic comparison of biomass-to-transportation fuels via pyrolysis, gasification, and biochemical pathways. *Fuel* **2010**, *89*, S29–S35. [CrossRef]
2. Agrawal, R.; Singh, N.R. Synergistic routes to liquid fuel for a petroleum-deprived future. *AIChE J.* **2009**, *55*, 1898–1905. [CrossRef]
3. Liu, C.; Wang, H.; Karim, A.M.; Sun, J.; Wang, Y. Catalytic fast pyrolysis of lignocellulosic biomass. *Chem. Soc. Rev.* **2014**, *43*, 7594–7623. [CrossRef] [PubMed]
4. Lee, J.; Xu, Y.; Huber, G.W. High-throughput screening of monometallic catalysts for aqueous-phase hydrogenation of biomass-derived oxygenates. *Appl. Catal. B Environ.* **2013**, *140–141*, 98–107. [CrossRef]
5. Ben, H.; Mu, W.; Deng, Y.; Ragauskas, A.J. Production of renewable gasoline from aqueous phase hydrogenation of lignin pyrolysis oil. *Fuel* **2013**, *103*, 1148–1153. [CrossRef]
6. Liu, D.; Li, G.; Yang, F.; Wang, H.; Han, J.; Zhu, X.; Ge, Q. Competition and Cooperation of Hydrogenation and Deoxygenation Reactions during Hydrodeoxygenation of Phenol on Pt(111). *J. Phys. Chem. C* **2017**, *121*, 12249–12260. [CrossRef]
7. Wu, X.; Ge, Q.; Zhu, X. Vapor phase hydrodeoxygenation of phenolic compounds on group 10 metal-based catalysts: Reaction mechanism and product selectivity control. *Catal. Today* **2021**, *365*, 143–161. [CrossRef]
8. Furimsky, E. Catalytic hydrodeoxygenation. *Appl. Catal. A Gen.* **2000**, *199*, 147–190. [CrossRef]
9. Caballero, A.; Holgado, J.P.; Gonzalez-delaCruz, V.M.; Habas, S.E.; Herranz, T.; Salmeron, M. In situ spectroscopic detection of SMSI effect in a Ni/CeO$_2$ system: Hydrogen-induced burial and dig out of metallic nickel. *Chem. Comm* **2010**, *46*, 1097–1099. [CrossRef]
10. Liu, L.; Zhou, F.; Wang, L.; Qi, X.; Shi, F.; Deng, Y. Low-temperature CO oxidation over supported Pt, Pd catalysts: Particular role of FeO$_x$ support for oxygen supply during reactions. *J. Catal.* **2010**, *274*, 1–10. [CrossRef]
11. Deleitenburg, C.; Trovarelli, A. Metal-support interactions in Rh/CeO$_2$, Rh/TiO$_2$, and Rh/Nb$_2$O$_5$ catalysts as inferred from CO$_2$ methanation activity. *J. Catal.* **1995**, *156*, 171–174. [CrossRef]
12. Tauster, S.J.; Fung, S.C.; Baker, R.T.K.; Horsley, J.A. Strong interactions in supported-metal catalysts. *Science* **1981**, *211*, 1121–1125. [CrossRef] [PubMed]
13. Fu, D.; Wu, X.; Cui, B.; Guo, Y.; Wang, H.; Han, J.; Ge, Q.; Zhu, X. Ru$_{0.05}$Ce$_{0.95}$O$_2$ Solid Solution Derived Ru Catalyst Enables Selective Hydrodeoxygenation of m-Cresol to Toluene. *ChemCatChem* **2021**, *13*, 4814–4823. [CrossRef]
14. Bertella, F.; Concepción, P.; Martínez, A. TiO$_2$ polymorph dependent SMSI effect in Co-Ru/TiO$_2$ catalysts and its relevance to Fischer-Tropsch synthesis. *Catal. Today* **2017**, *289*, 181–191. [CrossRef]
15. Labich, S.; Taglauer, E.; Knözinger, H. Metal–support interactions on rhodium model catalysts. *Top. Catal.* **2000**, *14*, 153–161. [CrossRef]
16. Fu, Q.; Wagner, T.; Olliges, S.; Carstanjen, H.D. Metal-Oxide interfacial reactions: Encapsulation of Pd on TiO$_2$ (110). *J. Phys. Chem. B* **2005**, *109*, 944–951. [CrossRef]
17. Zhang, J.; Zhang, M.; Jin, Z.; Wang, J.; Zhang, Z. Study of high-temperature hydrogen reduced Pt^0/TiO$_2$ by X-ray photoelectron spectroscopy combined with argon ion sputtering—Diffusion-encapsulation effect in relation to strong metal–support interaction. *Appl. Surf. Sci.* **2012**, *258*, 3991–3999. [CrossRef]
18. Tauster, S.J.; Fung, S.C.; Garten, R.L. Strong metal-support interactions. Group 8 noble metals supported on titanium dioxide. *J. Am. Chem. Soc.* **1978**, *100*, 170–175. [CrossRef]
19. Zhang, J.; Wang, B.; Nikolla, E.; Medlin, J.W. Directing Reaction Pathways through Controlled Reactant Binding at Pd-TiO$_2$ Interfaces. *Angew. Chem.* **2017**, *23*, 6694–6698. [CrossRef]
20. Huang, R.; Kwon, O.; Lin, C.; Gorte, R.J. The effects of SMSI on m-Cresol hydrodeoxygenation over Pt/Nb$_2$O$_5$ and Pt/TiO$_2$. *J. Catal.* **2021**, *398*, 102–108. [CrossRef]
21. Zhao, X.; Wu, X.; Wang, H.; Han, J.; Ge, Q.; Zhu, X. Effect of Strong Metal-Support Interaction of Pt/TiO$_2$ on Hydrodeoxygenation of m-Cresol. *ChemistrySelect* **2018**, *3*, 10364–10370. [CrossRef]
22. Resende, K.A.; Noronha, F.B.; Hori, C.E. Hydrodeoxygenation of phenol over metal supported niobia catalysts. *Renew. Energy* **2020**, *149*, 198–207. [CrossRef]
23. Lu, M.; Zhu, J.; Li, M.; Shan, Y.; He, M.; Song, C. TiO$_2$-Modified Pd/SiO$_2$ for Catalytic Hydrodeoxygenation of Guaiacol. *Energy Fuel* **2016**, *30*, 6671–6676. [CrossRef]
24. Newman, C.; Zhou, X.; Goundie, B.; Ghampson, I.T.; Pollock, R.A.; Ross, Z.; Wheeler, M.C.; Meulenberg, R.W.; Austin, R.N.; Frederick, B.G. Effects of support identity and metal dispersion in supported ruthenium hydrodeoxygenation catalysts. *Appl. Catal. A Gen.* **2014**, *477*, 64–74. [CrossRef]
25. Lu, M.; Du, H.; Wei, B.; Zhu, J.; Li, M.; Shan, Y.; Shen, J.; Song, C. Hydrodeoxygenation of Guaiacol on Ru Catalysts: Influence of TiO$_2$–ZrO$_2$ Composite Oxide Supports. *Ind. Eng. Chem. Res.* **2017**, *56*, 12070–12079. [CrossRef]
26. Boonyasuwat, S.; Omotoso, T.; Resasco, D.E.; Crossley, S.P. Conversion of Guaiacol over Supported Ru Catalysts. *Catal. Lett.* **2013**, *143*, 783–791. [CrossRef]
27. Chen, C.; Chen, G.; Yang, F.; Wang, H.; Han, J.; Ge, Q.; Zhu, X. Vapor phase hydrodeoxygenation and hydrogenation of m-cresol on silica supported Ni, Pd and Pt catalysts. *Chem. Eng. Sci.* **2015**, *135*, 145–154. [CrossRef]
28. Yan, P.; Kennedy, E.; Stockenhuber, M. Natural zeolite supported Ni catalysts for hydrodeoxygenation of anisole. *Green Chem.* **2021**, *23*, 4673–4684. [CrossRef]

29. Shu, R.; Xu, Y.; Ma, L.; Zhang, Q.; Chen, P.; Wang, T. Synergistic effects of highly active Ni and acid site on the hydrodeoxygenation of syringol. *Catal. Commun.* **2017**, *91*, 1–5. [CrossRef]

30. Nie, L.; de Souza, P.M.; Noronha, F.B.; An, W.; Sooknoi, T.; Resasco, D.E. Selective conversion of m-cresol to toluene over bimetallic Ni–Fe catalysts. *J. Mol. Catal. A Chem* **2014**, *388–389*, 47–55. [CrossRef]

31. Yang, F.; Libretto, N.J.; Komarneni, M.R.; Zhou, W.; Miller, J.T.; Zhu, X.; Resasco, D.E. Enhancement of m-Cresol Hydrodeoxygenation Selectivity on Ni Catalysts by Surface Decoration of MoOx Species. *ACS Catal.* **2019**, *9*, 7791–7800. [CrossRef]

32. Mortensen, P.M.; Grunwaldt, J.-D.; Jensen, P.A.; Jensen, A.D. Influence on nickel particle size on the hydrodeoxygenation of phenol over Ni/SiO$_2$. *Catal. Today* **2016**, *259*, 277–284. [CrossRef]

33. Shin, E.J.; Keane, M.A. Gas-phase hydrogenation/hydrogenolysis of phenol over supported nickel catalysts. *Ind. Eng. Chem. Res.* **2000**, *39*, 883–892. [CrossRef]

34. Zhang, X.; Yan, P.; Zhao, B.; Zhang, Z.C. Identification of electron-rich mononuclear Ni atoms on TiO$_2$-A distinguished from Ni particles on TiO$_2$-R in guaiacol hydrodeoxygenation pathways. *Catal. Sci. Technol.* **2021**, *11*, 297–311. [CrossRef]

35. Zhang, X.; Yan, P.; Zhao, B.; Liu, K.; Kung, M.C.; Kung, H.H.; Chen, S.; Zhang, Z.C. Selective Hydrodeoxygenation of Guaiacol to Phenolics by Ni/Anatase TiO$_2$ Catalyst Formed by Cross-Surface Migration of Ni and TiO$_2$. *ACS Catal.* **2019**, *9*, 3551–3563. [CrossRef]

36. Yang, F.; Liu, D.; Zhao, Y.; Wang, H.; Han, J.; Ge, Q.; Zhu, X. Size dependence of vapor phase hydrodeoxygenation of m-cresol on Ni/SiO$_2$ catalysts. *ACS Catal.* **2018**, *8*, 1672–1682. [CrossRef]

37. Mao, J.; Zhou, J.; Xia, Z.; Wang, Z.; Xu, Z.; Xu, W.; Yan, P.; Liu, K.; Guo, X.; Zhang, Z.C. Anatase TiO$_2$ Activated by Gold Nanoparticles for Selective Hydrodeoxygenation of Guaiacol to Phenolics. *ACS Catal.* **2016**, *7*, 695–705. [CrossRef]

38. Omotoso, T.O.; Baek, B.; Grabow, L.C.; Crossley, S.P. Experimental and First-Principles Evidence for Interfacial Activity of Ru/TiO$_2$ for the Direct Conversion of m-Cresol to Toluene. *ChemCatChem* **2017**, *9*, 2642–2651. [CrossRef]

39. Zhang, Y.; Liu, J.X.; Qian, K.; Jia, A.; Li, D.; Shi, L.; Hu, J.; Zhu, J.; Huang, W. Structure Sensitivity of Au-TiO$_2$ Strong Metal-Support Interactions. *Angew. Chem. Int. Ed.* **2021**, *60*, 12074–12081. [CrossRef]

40. Cui, B.; Wang, H.; Han, J.; Ge, Q.; Zhu, X. Crystal-phase-depended strong metal-support interactions enhancing hydrodeoxygenation of m-cresol on Ni/TiO$_2$ catalysts. *J. Catal.* **2022**, *413*, 880–890. [CrossRef]

41. Zhang, R.; Wei, A.; Zhu, M.; Wu, X.; Wang, H.; Zhu, X.; Ge, Q. Tuning reverse water gas shift and methanation reactions during CO$_2$ reduction on Ni catalysts via surface modification by MoOx. *J CO$_2$ Util* **2021**, *52*, 101678. [CrossRef]

42. Bui, V.N.; Laurenti, D.; Afanasiev, P.; Geantet, C. Hydrodeoxygenation of guaiacol with CoMo catalysts. Part I: Promoting effect of cobalt on HDO selectivity and activity. *Appl. Catal. B Environ.* **2011**, *101*, 239–245. [CrossRef]

43. Ferretto, L.; Glisenti, A. Surface acidity and basicity of a rutile powder. *Chem. Mater.* **2003**, *15*, 1181–1188. [CrossRef]

44. Chen, H.-Y.T.; Pacchioni, G. Role of Oxide Reducibility in the Deoxygenation of Phenol on Ruthenium Clusters Supported on the Anatase Titania (101) Surface. *ChemCatChem* **2016**, *8*, 2492–2499. [CrossRef]